Supplemental Information

Cloud Condensation Nuclei (CCN) Activity Analysis of Low-hygroscopicity Aerosols Using the Aerodynamic Aerosol Classifier (AAC)

Kanishk Gohil[1] and Akua Asa-Awuku[1,2]

[1]Department of Chemical and Biomolecular Engineering, University of Maryland, College Park, MD 20742, United States

[2]Department of Chemistry and Biochemistry, University of Maryland, College Park, MD 20742, United States

Correspondence: Akua Asa-Awuku (asaawuku@umd.edu)

Summary: This supplemental document contains the CCNC supersaturation calibration data, calculation of necessary AAC measurement parameters, methods for uncertainty analysis of number concentration data, description of the dynamic shape factor measurement method, and DMA-based CCN measurement data and associated uncertainties.

S1. CCN counter (CCNC) calibration

Dry particles are subjected to supersaturated conditions when passing through the CCNC column. The CCNC supersaturation is set by applying an axial temperature gradient for specified flow and pressure gradient within the CCNC column. Theoretically, the temperature gradient stays constant if the CCNC parameters are maintained constant. However, in practice there are fluctuations in the CCNC parameters which can cause deviations in the instrument supersaturation from the set supersaturation. These deviations in CCNC supersaturations were resolved by calibrating the CCNC. Calibration was performed by following the procedure described by Rose et al. (2008).

Table S1. $(NH_4)_2SO_4$ CCN Counter (CCNC) calibration data

Supersaturation Setting (%)	Calibrated Supersaturation (%)	Critical Dry Diameter (nm)
0.2	0.215	75.6 ± 2
0.3	0.308	61.7 ± 0.6
0.4	0.402	52.3 ± 0.6
0.5	0.493	45.5 ± 1
0.6	0.586	41.2 ± 0.4
0.8	0.771	34.7 ± 0.7
1.0	0.957	29.6 ± 0.6

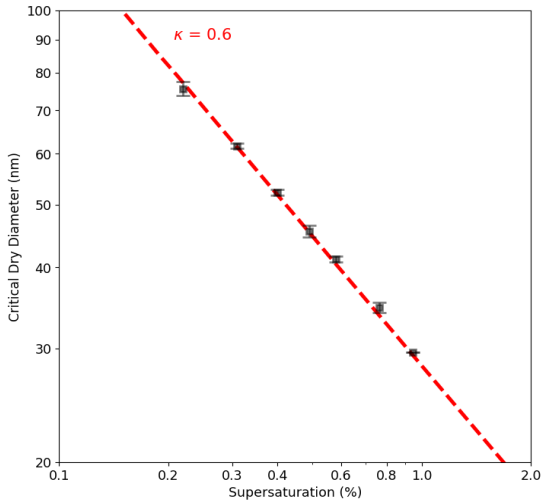

Figure S1. CCN counter (CCNC) calibration using $(NH_4)_2SO_4$ CCN measurements from DMA-based setup. The critical dry electrical mobility diameters are plotted against their respective instrument supersaturations and are overlayed against the $\kappa = 0.6$ line that corresponds to pure ammonium sulfate (Petters and Kreidenweis (2007)).

S2. Estimation of AAC measurement parameters

S2.1. Cunningham's Slip Correction Factor

Particles experience a drag force when they move along a fluid of given viscosity. Stokes' law provides a solution for estimating the viscous drag in laminar flow regimes where the Reynold's number << 1 (Crowder et al. (2002)). An underlying assumption in the estimation of this viscous drag is that there is no slip at the particle surface when particles move through the fluid. However, this assumption starts to

break down when the particle size becomes several times larger than the mean free path. In such cases, the drag force needs to be corrected for the slip to maintain a constant flow velocity. Cunningham derived a correction factor for the drag force, which is commonly expressed as a function of particle size (d) as follows,

$$C_c(d) = 1 + \frac{\lambda}{d} \cdot \left(\alpha_{C_c} + \beta_{C_c} \cdot \exp\left(-\gamma_{C_c} \cdot \frac{d}{\lambda}\right)\right) \quad \text{(S1)}$$

where $\alpha_{C_c} = 2.33$, $\beta_{C_c} = 0.966$ and $\gamma_{C_c} = 0.4985$ (Kim et al. (2005)). λ in Eq. (S1) is the mean free path of the surrounding gas particles which is estimated as follows (Eq. (S2)),

$$\lambda = \lambda_0 \cdot \left(\frac{T}{T_0}\right)^2 \cdot \left(\frac{P_0}{P}\right) \cdot \left(\frac{T_0 + S}{T + S}\right) \quad \text{(S2)}$$

where λ_0 is the air mean free path at the reference conditions of $67.3\ nm$, T is the air temperature in the classifier in K, T_0 is the reference temperature of $296.15\ K$, P is the air pressure in the classifier in Pa, P_0 is the reference pressure of $101325\ Pa$ and S is the Sutherland constant for air of $110.4\ K$.

S2.2. AAC Transfer Function Characterization

The AAC transfer function includes non-ideal particle behavior using the transmission efficiency (λ_Ω) and transfer function width factor (μ_Ω). The λ_Ω of the AAC is empirically determined using Eq. (S3) (Johnson et al. (2018)),

$$\lambda_\Omega = \lambda_D \cdot \lambda_e \quad \text{(S3)}$$

where λ_e is the entrance/exit transmission efficiency of the classifier, and λ_D is the diffusional transmission efficiency. λ_e for the AAC has been typically observed as 0.8. λ_D is given as,

$$\lambda_D = \begin{cases} 0.819e^{-11.5\delta_{dep}} + 0.0975e^{-70.1\delta_{dep}} + 0.0325e^{-179\delta_{dep}} & if\ \delta_{dep} \geq 0.007 \\ 1 - 5.5\delta_{dep}^{2/3} + 3.77\delta_{dep} + 0.814\delta_{dep}^{4/3} & if\ \delta_{dep} < 0.007 \end{cases} \quad \text{(S4)}$$

where δ_{dep} in Eq. (S4) is a size-dependent deposition parameter and is given as, $\delta_{dep}(d) = \frac{L_{eff} \cdot D(d)}{Q_a}$, such that L_{eff} is the effective deposition length of the AAC and has a value of 46m, $D(d)$ is the size-dependent diffusion coefficient of the particles, and Q_a is the aerosol flow rate.

S3. Uncertainty estimation for size-resolved counting and activation measurements

If N generally denotes the particle counts from a CPC or CCNC, and Q_a denotes the aerosol flow rate, the relative uncertainty in the measured particle concentration (ϵ_C) is determined from the relative counting uncertainty (ϵ_N) and the relative flow rate uncertainty (ϵ_{Q_a}) as follows (Moore et al. (2010)),

$$\epsilon_C^2 = \epsilon_N^2 + \epsilon_{Q_a}^2 \quad \text{(S5)}$$

*Particles are assume*d to be randomly distributed throughout the sample. Poisson statistics can be used to estimate ϵ_N as $\frac{\sigma_N}{N} \approx N^{-1/2}$. For the CCN counter (CFSTGC), the ϵ_{Q_a} is generally $\sim 4\%$. For the TSI CPC 3776, ϵ_{Q_a} is about 2%. The uncertainties in the particle concentrations can used to propagate the uncertainties in the size-resolved activation ratio $\left(R_a = \frac{C_{CCN}}{C_{CN}}\right)$. The uncertainties in size-resolved activation ratio $\left(\epsilon_{R_a}\right)$ can be denoted as,

$$\epsilon_{R_a}^2 = \epsilon_{C_{CNN}}^2 + \epsilon_{C_{CN}}^2 = \epsilon_{N_{CCN}}^2 + \epsilon_{N_{CN}}^2 + \epsilon_{Q_{CCN}}^2 + \epsilon_{Q_{CN}}^2 \quad \text{(S6)}$$

$$\epsilon_{R_a}^2 = N_{CCN}^{-1/2} + N_{CN}^{-1/2} + \epsilon_{Q_{CCN}}^2 + \epsilon_{Q_{CN}}^2 \quad \text{(S7)}$$

Eq. (S6) can be simplified to Eq. (S7). Under standard experimental conditions, for most atmospherically relevant CN concentrations, $\epsilon_{C_{CN}}$ is 7% or less, while $\epsilon_{C_{CCN}}$ is less than 17%. The subsequent ϵ_{R_a} is less than 18% (Moore et al. (2010)).

S4. Shape factor measurements

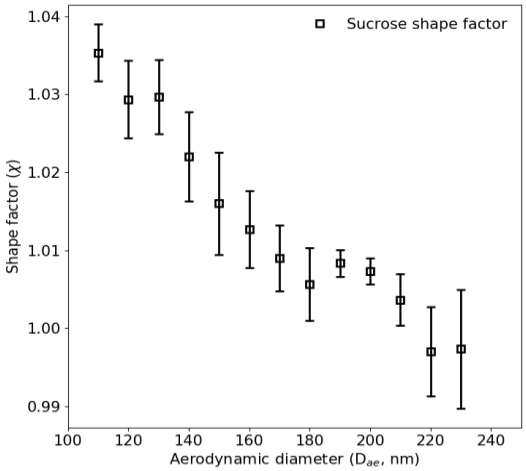

Figure S2. Sucrose dynamic shape factor data for sucrose, collected using an AAC-DMA setup (Tavakoli and Olfert (2014)). The size-resolved shape factor is plotted against the aerodynamic diameter measurements of sucrose. Shape factor relates aerosol density with the particle size and was used to derive volume equivalent diameters corresponding to the respective aerodynamic diameters (details in sections 3 and 4 of main text). The above figure shows that the shape factor of sucrose is close to 1 over a range of sizes, which implies that sucrose particles are mostly spherical.

S5. DMA-CCNC measurements

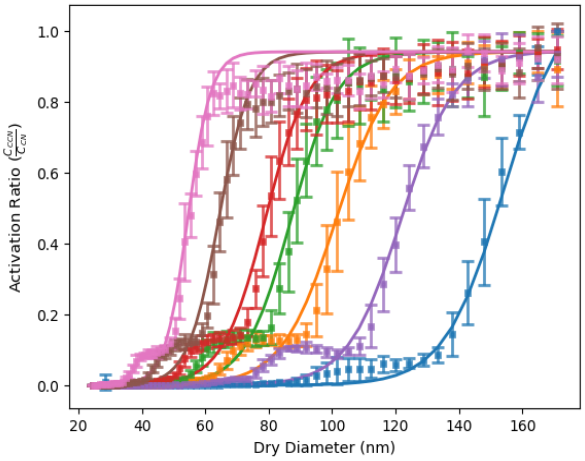

Figure S3. Size-resolved activation data of sucrose determined using CCN measurements using a DMA-based setup. The activation ratios are shown with respect to electrical mobility diameters.

Table S2. Sucrose DMA-based CCN Activation Data. Uncertainties in Critical Dry Diameters Using Electrical Mobility Measurements from a DMA-based Setup

Instrument Supersaturation (%)	**Critical Dry Diameter (nm)**	**Uncertainties in Critical Dry Diameters** (%)
0.215	153.3	±7.42
0.308	122.3	±7.11
0.402	99.1	±6.91
0.493	87.2	±6.75
0.586	78.2	±6.67

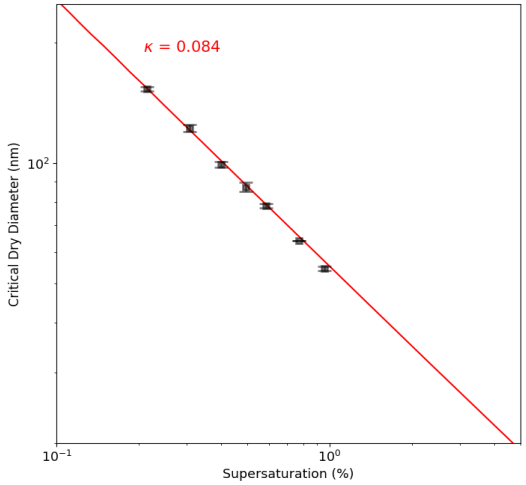

Figure S4. CCN measurements of sucrose from DMA-based setup. The activation measurements overlayed with $\kappa = 0.084$ line which corresponds to pure (ideal) sucrose.

Supplemental References

Crowder, T. M., Rosati, J. A., Schroeter, J. D., Hickey, A. J., & Martonen, T. B.: Fundamental effects of particle morphology on lung delivery: predictions of Stokes' law and the particular relevance to dry powder inhaler formulation and development, pharmaceutical research, 19, 239-245, 2002.

Johnson, T. J., Irwin, M., Symonds, J. P., Olfert, J. S., and Boies, A. M.: Measuring aerosol size distributions with the aerodynamic aerosol classifier, Aerosol Science and Technology, 52, 655–665, 2018.

Kim, J. H., Mulholland, G. W., Kukuck, S. R., and Pui, D. Y.: Slip correction measurements of certified PSL nanoparticles using a nanometer differential mobility analyzer (nano-DMA) for Knudsen number from 0.5 to 83, Journal of Research of the National Institute of Standards and technology, 110, 2005.

Moore, R. H., Nenes, A., and Medina, J.: Scanning mobility CCN analysis—A method for fast measurements of size-resolved CCN distributions and activation kinetics, Aerosol Science and Technology, 44, 861–871, 2010.

Petters, M. D. and Kreidenweis, S. M.: A single parameter representation of hygroscopic growth and cloud condensation nucleus activity, Atmospheric Chemistry and Physics, 7, 1961–1971, 2007.

Rose, D., Gunthe, S., Mikhailov, E., Frank, G., Dusek, U., Andreae, M. O., and Pöschl, U.: Calibration and measurement uncertainties of a continuous-flow cloud condensation nuclei counter (DMT-CCNC): CCN activation of ammonium sulfate and sodium chloride aerosol particles in theory and experiment, Atmospheric Chemistry and Physics, 8, 1153–1179, 2008.

Tavakoli, F. and Olfert, J. S.: Determination of particle mass, effective density, mass–mobility exponent, and dynamic shape factor using an aerodynamic aerosol classifier and a differential mobility analyzer in tandem, Journal of aerosol science, 75, 35–42, 2014.

Yao, Q., Asa-Awuku, A., Zangmeister, C. D., and Radney, J. G.: Comparison of three essential sub-micrometer aerosol measurements: Mass, size and shape, Aerosol Science and Technology, 54, 1197–1209, 2020.